SAND2017-11517C

Inverse Methods for Characterization of Contact Areas in Mechanical Systems

Matthew Fronk
Department of Material Engineering
Georgia Institute of Technology
Atlanta, GA

Kevin Eschen
Department of Mechanical Engineering
University of Minnesota, Twin Cities
Minneapolis, MN

Kyle Starkey
Department of Mechanical Engineering
Purdue University
West Lafayette, IN

Robert J. Kuether
Sandia National Laboratories
Albuquerque, NM

Adam Brink
Sandia National Laboratories
Albuquerque, NM

Timothy Walsh
Sandia National Laboratories
Albuquerque, NM

Wilkins Aquino
Department of Civil and Environmental Engineering
Duke University
Durham, NC

Matthew Brake
Department of Mechanical Engineering
Rice University
Houston, TX

ABSTRACT

In computational structural dynamics problems, the ability to calibrate numerical models to physical test data often depends on determining the correct constraints within a structure with mechanical interfaces. These interfaces are defined as the locations within a built-up assembly where two or more disjointed structures are connected. In reality, the normal and tangential forces arising from friction and contact, respectively, are the only means of transferring loads between structures. In linear structural dynamics, a typical modeling approach is to linearize the interface using springs and dampers to connect the disjoint structures, then tune the coefficients to obtain sufficient accuracy between numerically predicted and experimentally measured results. This work explores the use of a numerical inverse method to predict the area of the contact patch located within a bolted interface by defining multi-point constraints. The presented model updating procedure assigns contact definitions (fully stuck, slipping, or no contact) in a finite element model of a jointed structure as a function of contact pressure computed from a nonlinear static analysis. The contact definitions are adjusted until the computed modes agree with experimental test data. The methodology is demonstrated on a C-shape beam system with two bolted interfaces, and the calibrated model predicts modal frequencies with $< 3\%$ total error summed across the first six elastic modes.

Keywords: Modal analysis; linearized contact; multi-point constraints; model updating; mechanical interfaces

1 INTRODUCTION

Frictional joints are common in mechanical designs as a cost effective means of building up easy-to-manufacture substructures. However, the effect that frictional interfaces add to the mechanical response of the structure are complex and require advanced computational and experimental techniques to characterize. Nonlinear stiffness and damping are two salient examples of the complicated phenomena that arise due to joints in structures. Consequently, it is important to understand joint interactions at

a fundamental level to more accurately account for them in models and thus better inform design making decisions. This study aims to update the contact conditions to identify the true contact area of the interface(s) in a linearized computational structural dynamics model of a jointed structure using low-level, linear test data. The calibration routine aims to match computational and experimental modal frequencies by updating contact definitions at the element level in the finite element model as a function of the numerically computed contact pressure. The results of this analysis provide greater insight into the contact area that occurs at frictional interfaces of bolted connections and confidence in the method developed to calibrate numerical models to modal test data.

The calibration of computational models with experimental data, commonly known as model updating, has been well studied by the engineering community. Mottershead and Friswell provide an overview as it relates to vibration testing in [1]. Additionally, Ewins [2] discusses challenges to model updating, emphasizing the need to incorporate nonlinearities and the complexities introduced by joints. A common approach to matching modal test data to finite element models of jointed structures is to linearize the interface with springs, masses, and/or dampers and vary the parameters until an acceptable level of agreement is reached [3−6]. Other approaches of model updating with joints include geometric parameters [7] and solving a reduced order polynomial identified from both computational and modal data [8]. In a more recent study conducted by Adel et al [9], the mechanical properties of a "doubly-connective layer" in a computational model of a lap joint were optimized to match modal test data. In experimental settings, direct measurements of pressure patches have included electrical measurements that capture time-dependent patches [10] and ultrasonic techniques [11]. Furthermore, many computational modeling techniques have been developed that capture *nonlinear* joint behavior [12−15], however this is beyond the scope of this work.

This paper presents a model updating scheme to determine the contact area at a linearized bolted interface joining two C-shaped beams. Experimentally measured modal frequencies are compared to those generated with a finite element (FE) model of the structure. The first step in the inverse method is to solve a nonlinear static preload analysis of the FE model with the appropriate torque/preload force on the bolt to obtain the contact pressure at the interface. A single parameter, namely the cut-off pressure, is then varied to determine the contact definitions governing each element in the interface. The cut-off pressure is a continuous variable that defines the following condition: elements with contact pressures above this value are considered stuck (i.e. welded together), and elements below this value can either slide or are unconstrained. With the updated contact definition for a given cut-off pressure, the modal frequencies are re-computed and compared to the experimentally measured modes using a least-squares error metric. An optimal solution is found once this objective function is minimized.

A brief outline of the paper is as follows: Section 2 details the model updating procedure. Section 3 overviews the system geometry, experimental data acquisition procedure, and modal characteristics of the beam system. Section 4 presents results of the static preload analysis that determines the contact pressure distribution on the interface, as well as the results from the model updating routine and a discussion on the accuracy. The conclusions from this research are presented in Section 5.

2 SINGLE PARAMETER INVERSE METHOD

2.1 INPUTS & OUTPUTS

This work proposes a single parameter inverse method as a model updating procedure to adjust the contact definitions of element faces at the interface of a jointed structure with the goal of finding modal solutions that best match experimentally-measured modes. The only parameter that is adjusted is the cut-off pressure associated with the contact pressures computed from a nonlinear static preload analysis. An inverse method has the objective of adjusting the unknown system parameters (i.e. contact definitions) to agree with known inputs and outputs. This objective is in contrast to forward problems, in which the output is determined for known system parameters and inputs.

The inverse problem has multiple inputs associated with the finite element model. The geometry of the structure is required to develop a finite element mesh, and the material properties, such as the density ρ and the modulus of elasticity E, are required to develop the discretized equations of motion. The normal contact pressure distribution is a model input that is computationally-obtained from a static preload analysis using a (presumably) known preload force from the tightened bolt. The single parameter inverse method uses normal contact pressure information to update the contact definition in the interface. As described in Section 4.1, commercial finite element solvers can be used to obtain normal contact force data on a single node, f_{node}. Consequently, these nodal forces can then be translated into element pressures, p_{elem}, by averaging the nodal pressures associated with each element face. In addition to the aforementioned inputs, the single parameter inverse method uses output data that is observable from both the experimental and computational system. This research relies on the modal solutions computed from the linearized finite element model, and the modes extracted from test data on the physical hardware.

2.2 CONTACT DEFINITIONS

Within the node-to-face constraints employed in this research, three linearized contact conditions are possible: stuck, sliding, and no contact. The no contact condition allows for deformation of the faces without restricting any degree of freedom. Under this condition, there are no normal forces or tractions transferred from one face onto another and interpenetration may occur. A level of constraint is added in the sliding contact condition, which restricts normal displacements on the master and slave node/face pair to be equal, but allows for tangential motion. This contact definition resembles a Coulomb friction definition with a friction coefficient $\mu = 0$. All degrees of freedom in the interface are constrained when using the stuck contact definition, not allowing for any relative motion between contacting node/face pair. A Coulomb friction model is employed during the nonlinear preload analysis to capture the appropriate contact pressures, but is not used for the linearized modal analysis.

2.3 CONTACT AREA OPTIMIZATION

The single parameter from which this inverse method derives its name from is the cut-off pressure, p_l, used to adjust the contact definitions along the interface. This free variable is used as the sole optimization parameter for the model updating procedure. The numerically calculated element pressures, p_{elem}, from the nonlinear static analysis are determined, and the contact definitions are enforced based on whether the pressures are above or below p_l. Two different updating schemes are described in the following paragraphs and compared later in Section 4.2.

The first implementation of the single parameter inverse method utilizes all three of the possible contact conditions: stuck, sliding, and no contact. Each element face with a pressure equal to numerical zero receives a no contact condition. The sliding contact condition is assigned to element face pressures that are below the cut-off pressure, p_l, but greater than numerical zero. Every element with pressures above or equal to p_l is rigidly tied using the stuck condition. These logic statements are described in Equations 1 - 3.

$$p_{elem} \leq 0 \rightarrow \text{No Contact} \tag{1}$$

$$0 < p_{elem} < p_l \rightarrow \text{Sliding Contact} \tag{2}$$

$$p_{elem} \geq p_l \rightarrow \text{Stuck Contact} \tag{3}$$

The second implementation of the single parameter inverse method is similar to the first, but instead only permits the stuck and no contact definitions. These logic statements are described in Equations 4 - 5. Now the element faces with a contact pressure between zero and the cut-off pressure p_l are also assigned a no contact condition. Note that this contrasts that of the first implementation, which assigns sliding contact to elements within this range. The contact condition for elements with pressures above p_l are defined to be in stuck contact.

$$p_{elem} < p_l \rightarrow \text{No Contact} \tag{4}$$

$$p_{elem} \geq p_l \rightarrow \text{Stuck Contact} \tag{5}$$

Based on these contact definitions for a given inverse approach and value of p_l, the multi-point constraints within the finite element model end up modifying the discretized mass and stiffness matrices. An eigenanalysis is formulated for a given constrained system and solved using a commercial finite element solver. The eigenanalysis equation is described as,

$$\left(\mathbf{K} - \omega_{n,m}^2 \mathbf{M}\right) \phi_m = \mathbf{0} \tag{6}$$

where $\mathbf{K}$ and $\mathbf{M}$ correspond to the constrained stiffness and mass matrices, respectively. The index m corresponds to the mode number associated with a computed modal frequency, $\omega_{n,m}$, and mode shape, ϕ_m. These equations are solved using Lanczos-method, a computationally efficient pre-defined method found in most commercial finite element solvers.

The optimal value of p_l is sought for either implementation of the single parameter inverse method, as shown later in Section 4.2. This is achieved by defining an objective function that is a measure of the error between the experimentally measured and numerically

calculated modal frequencies. This error metric is defined as the scalar, $|e|$,

$$|e| = \sqrt{\sum_{m=1}^{N} \left(\frac{\omega_{n,m,exp} - \omega_{n,m}}{\omega_{n,m,exp}} \right)^2}, \tag{7}$$

where the number of the elastic modes, N, are defined by the experimentally-obtained modal frequency of a specific mode, $\omega_{n,m,exp}$, and the numerically-calculated frequency, $\omega_{n,m}$, as provided in Equation 6. The minimization of this objective function yields a single cut-off pressure p_l at which the modal frequencies of the modeled system most closely match those of the experiment.

3 SYSTEM DESCRIPTION

3.1 EXPERIMENTAL SET-UP

The system considered in this study consists of two identical C-shaped beams brought into contact through two bolted joints on each end. A schematic of the geometry is provided in Figure 1. There are two general regions on each $508\ mm$ long beam: the slender center portion with cross-sectional dimensions of $31.8\ mm \times 9.65\ mm$ and the elevated surfaces on the ends of the beams with the cross-sectional dimensions of $31.8\ mm \times 12.7\ mm$. The beams are bolted together using 5/16"-24 bolts, nuts, and washers at each end of the beam assembly. The interfaces were machined to be nominally flat with a surface roughness average of Ra $= 8$. The Ra value corresponds to the average height deviations from the mean line along a given surface. Holes were machined through the slender, center portions of the beams to enable the attachment of fishing line and soft bungee cords to approximate free-free boundary conditions.

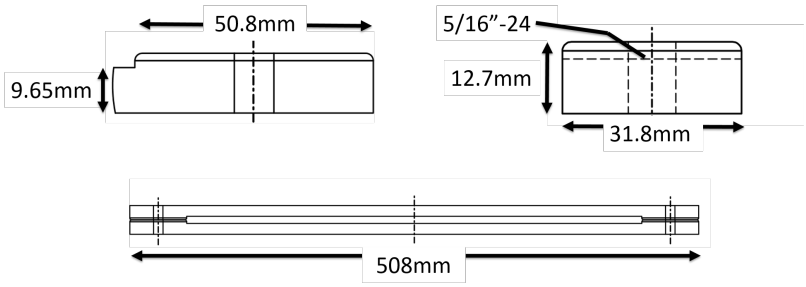

Figure 1: Beam system drawing with important dimensions

Experimental modes of the beam assembly were collected from low-level impact excitations to supply the reference data to the inverse method. To mimic free-free boundary conditions, two sets of fishing line looped into the beam through holes to an overhead fixture. Figure 2 displays a labeled experimental set-up, identifying the locations of the boundary conditions (i.e. low stiffness springs) and accelerometers. Four points were identified along the beam structure to place the accelerometers to capture the expected mode shapes. Furthermore, the beam was impulsively struck at approximately every $2.5\ cm$ along the beam in a roving hammer test to fully capture the modal responses. The test yielded linear results with impacts at approximately $15\ N$ in the z and y directions. These directions correspond to a Cartesian coordinate system in which x and y define perpendicular directions along the beam's height and length, respectively, and z defines the direction along the beam's thickness.

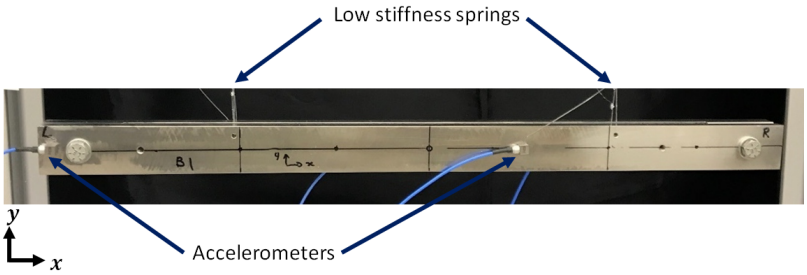

Figure 2: Experimental set-up to collect measurements for model updating

The accelerometer data collected in the experiments was used to estimate the frequency response functions (FRFs) from which the first six elastic vibration modes were fitted. There were a total of six rigid body modes present in the FRFs with modal frequencies $< 10\ Hz$ due to the low-stiffness boundary conditions that were not extracted or used throughout this research. The first six elastic modes occur within the $1000\ Hz$ frequency bandwidth of interest. Table 1 shows the natural frequencies from the test data, as well as the mode shapes of the corresponding modes predicted by the FE model later in Section 3.2. The mode shapes from the computational model imposed fully stuck contact conditions at all elements on each of the flat interfaces. For each of the modes, the finite element model overpredicts the natural frequencies of interest due to the fact that the interface is overconstrained with all elements fully stuck. This data comparison serves as the upper boundary of the model predictions.

TABLE 1: Comparison between test and analysis for the first six elastic modes of the C-shaped beam system

Mode Number	FEA Natural Frequency [Hz]	Experimental Natural Frequency [Hz]	Mode Shape
7	271	258	
8	338	331	
9	483	478	
10	571	567	
11	744	710	
12	892	855	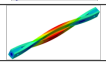

3.2 FINITE ELEMENT MODEL

A finite element model of the C-shape beam system was developed for the inverse study consisting of approximately 47,500 8-noded hexahedral elements. The bolt, washer and nut subassembly was simplified with beam elements (25 across the bolt length) whose ends are rigidly spidered to the surface corresponding the area underneath the washers. It is assumed that there is no slip occuring at these interfaces. The beam elements running through the bolt holes add both the longitudinal and bending stiffness associated with the actual bolts. Rigid spiders branching out from the ends of the beam elements to the surrounding nodes in the beam structures model the contact interface of the washers. A view of the beam element and rigid spider assembly is pictured in Figure 3. Both the models of the bolt and the C-shape beams use nominal material properties of structural steel with density $8000\ kg/m^3$, modulus of elasticity $194\ GPa$, and Poisson's ratio 0.29.

Finite element discretizations of structures with local interface kinematics in structural dynamics applications often require detailed models with fine mesh resolution. The balance between the appropriate mesh size and computational expense is a major challenge in computational modeling and is vital to achieving accurate results for applications when a large number of analysis iterations are needed, such as inverse methods. The beam mesh density is chosen to obtain converged results while keeping the mesh as coarse as possible. A total of approximately 50,000 8-noded hexahedral elements are used for the most refined solution, which correlates to approximately 2,000 element faces on the contact surfaces shown in Figure 4. The sensitivity of the computational modal analysis results for the first five elastic modes is summarized in Table 2. Two bounding contact conditions are presented in this table: a fully stuck interface and a predominantly no contact interface with stuck elements in a small annulus around the through hole. Mode shapes and natural frequencies under both bounding contact conditions do not vary appreciably as the number of nodes changes between 7,835 and 31,798. These results assure that the optimal mesh can be based purely on its resolution of local contact phenomena and the associated computational expense.

The normal mode calculations from the FE model for the two bounding contact conditions provides insight into the sensitivity of individual modes to interface contact definitions. For example, mode 10 is a bending deformation in the y-direction and does not appear to load the interface. This shape is especially insensitive (deviation below 1%) to the applied contact conditions. Due to this insensitivity, the 10^{th} mode provides a basis for the material properties to be calibrated. A match between the experimentally-obtained and numerically-calculated modal frequency for the 10^{th} mode occurs for a modulus of elasticity of $181\ GPa$. While the masses of the accelerometers used in the experimental set-up are small in comparison to the mass of the beams, they contribute to the system response depending on their position within the beam system set-up. In particular, the accelerometers positioned on the beam, as displayed in Figure 2, have a nontrivial effect on the numerical solution for specific modes (approximately $5\ Hz$ deviation

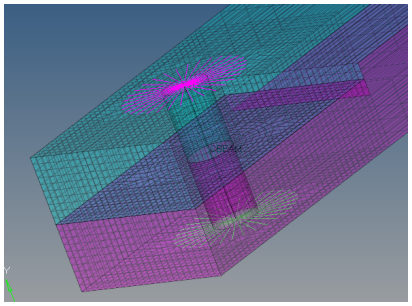

Figure 3: FE modeling of washers and bolt

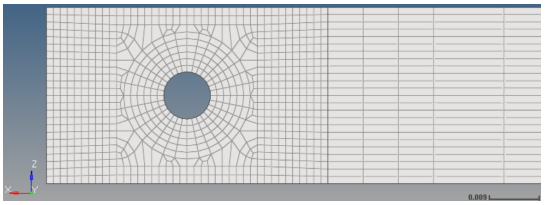

Figure 4: Optimal mesh to balance resolution with computational expense

in the 7th and 11th modes) and thus are modeled as point masses with mass $m = 0.02\ kg$.

4 RESULTS

4.1 STATIC PRELOAD ANALYSIS

The single parameter inverse method uses the computed pressure distribution at the interfaces from a nonlinear static preload analysis subject to a given bolt torque/preload force. These solutions are obtained using Altair's Optistruct implicit solver, which incrementally applies loads and iteratively solves equlibrium equations until certain convergence criteria are met (e.g. displacement, load, work). In the nonlinear static FE model, frictional contact between the beam surfaces is accounted for using Coulomb friction and the penalty method. A static friction coefficient of $\mu = 0.3$ governs the tangential forces between the metallic surfaces. The penalty stiffness at each element is set to the software's default value. Contact pressure results from simulations at various bolt torque levels reveal that the friction coefficient does not affect the pressure distribution shape (i.e. only the pressure magnitudes are scaled proporational to the bolt force). This observation is consistent with receding contact theory for flat-on-flat surfaces with similar materials [16]. While the experimental setup employs low-stiffness supports to mimic free-free boundary conditions, the computational model does not enforce such restraints and uses purely free-free boundary conditions to ensure the bolt loads transfer directly into the interface. The inertial relief option is applied to the static simulation to prevent rigid body motion.

For the preload step, the finite element software applies bolt pretensions instead of torques. Since the experimental hardware measured the bolt load using a torque wrench, an appropriate constitutive relationship was used to map the specified torque level to a corresponding axial force. One well known relationship, known as the Motosh equation [17], relates torque to bolt force as,

$$T = F\left(\frac{P}{2\pi} + \frac{\mu_t r_t}{cos(\beta)} + \mu_n r_n\right) \tag{8}$$

where T denotes the applied bolt torque, F is the axial force supplied by the bolt, P is the thread pitch, μ_t is the coefficient of friction between the nut and bolt threads, r_t is the effective contact radius of the threads, β is the half-angle of the threads, μ_n is the coefficient of friction between the face of the nut and the upper surface of the joint, and r_n denotes the effective radius of contact between the nut and joint surface. Results from applying Equation 8 to torque values of 10.2, 16.9, and 25.1 $N - m$ are presented in Table 3. These torque values correspond to the values at which the pressure film measurements were taken on the experimental hardware.

TABLE 2: Mesh sensitivity comparison of the first six elastic modal frequencies for bounding contact conditions

#-Nodes	#-Elements	Fully Stuck	Hole-Nodes Stuck	7^{th} mode [Hz]	8^{th} mode [Hz]	9^{th} mode [Hz]	10^{th} mode [Hz]	11^{th} mode [Hz]	12^{th} mode [Hz]
7835	1152		X	178	332	501	514	515	594
31798	5702		X	177	332	501	513	515	594
7835	1152	X		287	353	502	594	787	957
31798	5702	X		287	353	502	594	788	957

TABLE 3: Bolt torque to axial pretension conversions

Exp. Torque [N-m]	Motosh Force [kN]
10.2	8.6
16.9	14.3
25.1	21.2

A side profile view of the deformations near one of the bolted joints resulting from the static preload analysis is presented in Figure 5. Note that the flat interfaces are in contact near the bolt hole but bend away (or recede) from each other far away from it. The deformation has been amplified to reveal the characteristics of the deformation. Contact pressure profiles for the beam structure subjected to $21.2\ kN$ of pretension are shown in Figure 6, which displays contact pressure contours throughout the interface. The plot in Figure 7 shows a line slice of the interface contact pressure along the horizontal centerline in Figure 6. Notice that the contact pressure is highest around the bolt hole (region between the blue dashed lines in Figure 7) and decreases in concentric rings outward from the bolt location.

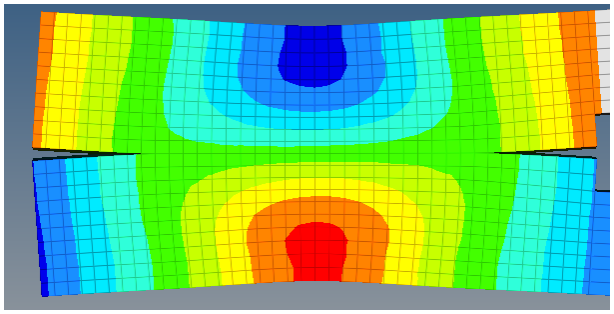

Figure 5: Deformed side view of the structure subjected to bolt pretension of $21.2\ kN$; colorbar corresponds to vertical displacements

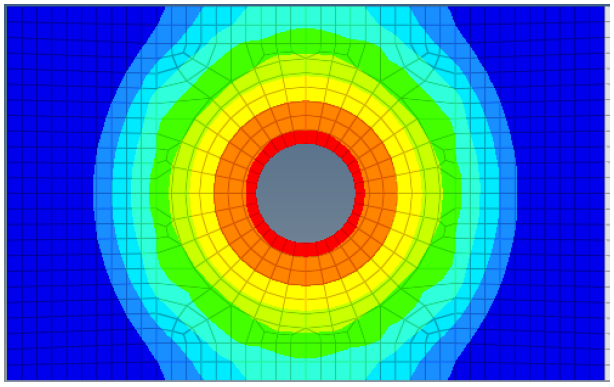

Figure 6: Normal contact pressure profile in the FE beam subjected to bolt pretension of $21.2\ kN$

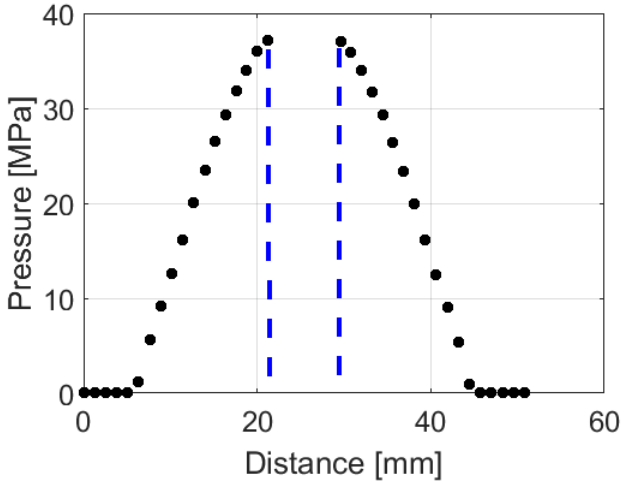

Figure 7: Interface contact pressure along the horizontal centerline in a beam subjected to bolt pretension of $21.2\ kN$

To assess the validity of the static pressure simulations, the results are compared with digitized pressure film measurements taken in the actual beam hardware when the bolts were tightened to $25.1\ N-m$. Both low (range of 2.4 to $9.7\ MPa$) and medium (range of 9.7 to $49\ MPa$) scale pressure films were used and these results are shown in Figure 8. Note that both pressure films exhibit saturation as evidenced by the red colored regions, indicating the measured pressure exceeds the films upper boundary of either 9.7 MPa or $49\ MPa$. Consequently, the low pressure film proves useful for reading pressures away from the bolt hole while the medium pressure film better captures the pressure values near the bolt hole.

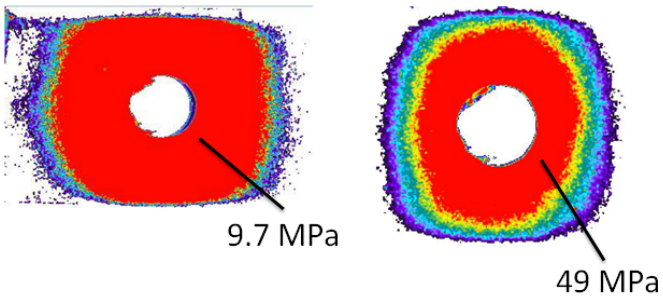

Figure 8: Low (left) and medium (right) film measurements taken in the actual beam assembly

Due to the uncertainty in the analytical relationship between axial pretension force and bolt torque, the bolt pretension values were calibrated in the FE model to match experimentally measured peak pressure values obtained from the pressure film measurements. The results from the medium pressure film in Figure 8 are used since the peak pressure values are visible and better capture the maximum contact pressure that occurs around the bolt hole. The results of the calibration process are presented in Figure 9. Note that the FE model achieves a peak pressure value of approximately $49\ MPa$ when using a $28.0\ kN$ pretension force. This agrees well with the peak pressure value measured by the medium pressure film measurement in Figure 8, but requires a force that is 32 percent larger than the value predicted by the Motosh Equation in Equation 8. It is important to note that there is considerable uncertainty associated with mapping a torque to an bolt pretension using closed form analytical solutions [18], thus highlighting the importance of measuring the contact pressures experimentally.

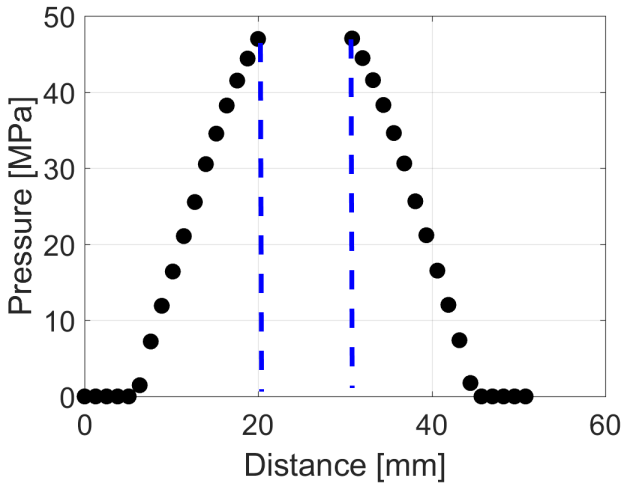

Figure 9: Interface contact pressure along the horizontal centerline in a beam subjected to calibrated bolt pretension of $28.0\ kN$

4.2 MODEL UPDATING RESULTS

This subsection compares the results for the two versions of the single parameter inverse method described in Section 2.3. Due to the discrete nature of the pressures predicted by static analysis at a finite number of element faces, a given value of p_l would produce a zero or discontinuous derivative. This means that there are only discrete changes in cut-off pressure values that would alter the contact definition at the interface. Standard gradient-based optimizers require a continuous parameter space with continuous derivatives and hence could not be used in this work. The results presented in this subsection are obtained by sampling the cut-off pressures at the discrete values obtained from all the interface elements in the static preload analysis.

The results from the first implementation are shown in Figure 10, such that the sliding condition is utilized for pressure below the cut-off value but greater than zero. This plot displays the modal frequencies of modes 7 through 12, relating to the first six elastic modes, computed at discrete cut-off pressures, p_l. The dashed-lines correspond to the modal frequencies measured from experiment, and the solid lines correspond to the modes from the FE model. A given mode can be considered optimal when the solid line crosses

the dashed experimental line. The first observation made from this plot is that modes 7, 8, 9, 10 and 11 show little sensitivity to the contact definition associated with p_l. Recall that modes 8 and 9 are bending modes in the xy-plane, as seen in Table 1. Notice that the interfaces do not bend when the beam deforms in the shapes of these modes. As a result, the joint is not loaded significantly and is insensitive to changes in the contact conditions. Mode 10 is a similar bending mode in the xz-plane, which, similarly to modes 8 and 9, has minimal influence on the shear loads in the joint. Modes 7 and 11 are clapping modes in the xy-plane leading to an opening and closing of the contact surface. While the sliding contact definition can capture relative displacements tangential to the contact surface, it restricts relative displacements normal to the contact surface, resulting in an essentially stuck contact condition for these two clapping modes. In contrast, mode 12 is highly sensitive to its contact definition as the contact surface around the bolt experiences significant shearing for this mode and the sliding contact definition captures this motion well. This mode is considered optimal at a cut-off pressure of about $18\ MPa$. These results reveal that not all of the modes are sensitive to the change in contact condition, and there is still a significant amount of error observed in the modes of interest (i.e. modes 7 and 11 in particular).

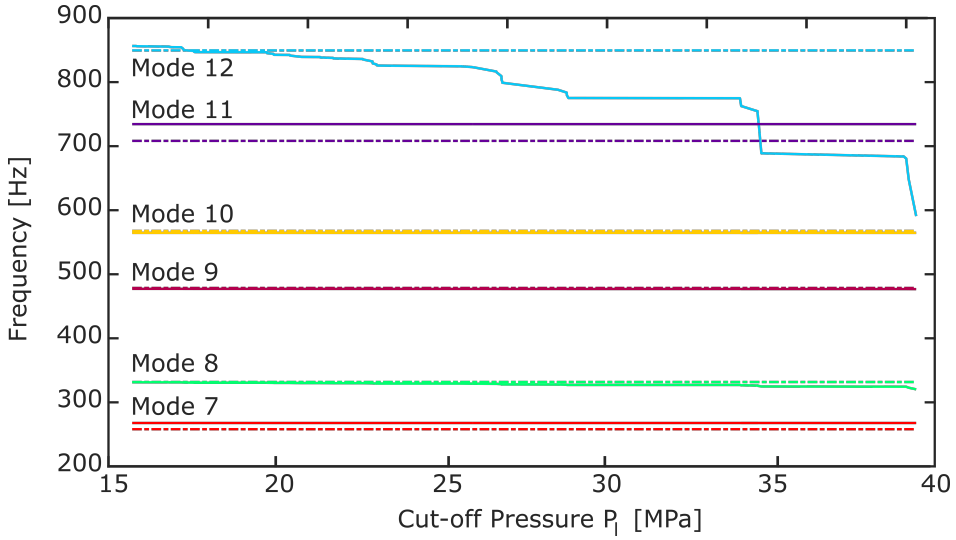

Figure 10: Modal frequencies computed at various cut-off pressures using three contact conditions

The second implementation of the single parameter inverse method overcomes the limitations observed with the two clapping modes 7 and 11. Figure 11 displays the modal frequencies for the first six elastic modes for the second implementation for discrete values of cut-off pressure p_l. In this case, modes 8, 9, and 10 are still not sensitive to the contact definitions due to the reasons previously discussed. Mode 12 is still highly sensitive since the interface is allowed to rotate and shear more or less with changing cut-off pressures. This mode crosses the experimental line now at a higher cut-off pressure, around $23\ MPa$, compared to the previous case at $18\ MPa$. The biggest improvement from the second implementation was seen with the sensitivity of modes 7 and 11, which were the clapping modes in the xy-plane. Since the change in p_l now releases the tangential *and* normal constraints, the stiffness of the clapping modes is able to decrease with increasing p_l. Now modes 7 and 11 cross the experimental value at around $22\ MPa$ and $24\ MPa$, respectively. The change from sliding to no contact conditions now have all of the sensitive modes of interest cross at nearly the same pressure, suggesting a better solution is obtainable with the second approach.

The individual mode representations in Figures 10 and 11 give insight into the ability of the inverse method to capture true contact area at the bolted joint interface. The frequency errors are quantified in Figure 12 by evaluating the objective function in Equation 7 at each cut-off pressure p_l. The three contact condition implementation is shown in blue while the two condition case is in green. The method using two contact conditions provides the optimal result with an error of $|e| < 3\%$ at a cut-off pressure of $p_l = 23\ MPa$, and the contact area of this is shown in the subplot within Figure 12. The method using three contact conditions achieves a minimal error of $|e| = 6.5\%$ at $p_l = 17\ MPa$. The low error associated with the second implementation (i.e. two contact conditions) highlights the insight that can be gained from understanding how the mode shapes load the interface, and how to assign realistic contact definitions.

The objective function plot in Figure 12 reveals the discrete nature of the single parameter p_l. The objective function is clearly discontinuous and would not work with gradient-based optimization algorithms. This problem was small enough that sampling the design space was completed in less than 24 hours on a standard laptop computer. The sampling approach could be parallelized with high performance computing resources, but this was not necessary for this research. These results reveal a successful proof-of-concept that the linearized structural dynamics model can be calibrated to test data by simply adjusting the contact area in a

bolted interface by systematically adjusting the cut-off pressure from the results obtained from a nonlinear static preload analysis.

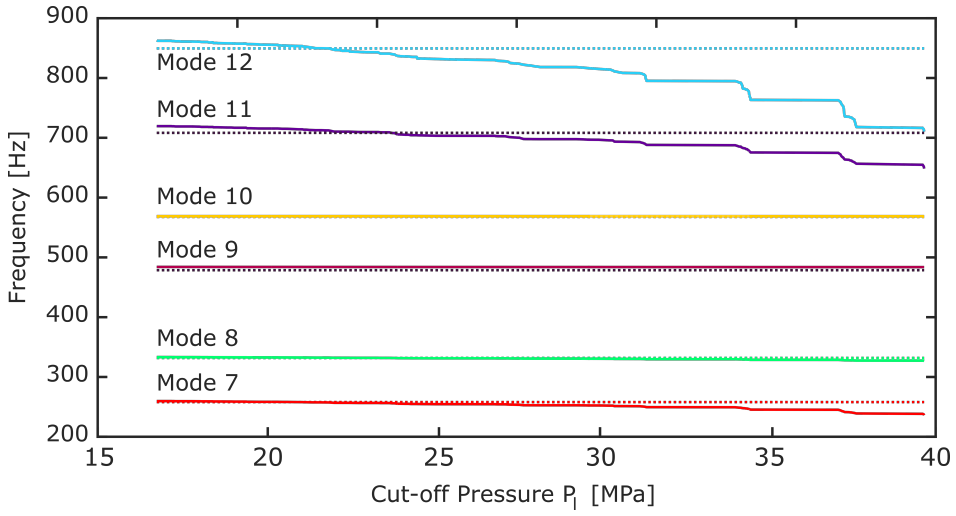

Figure 11: Modal frequencies computed at various cut-off pressures using two contact conditions

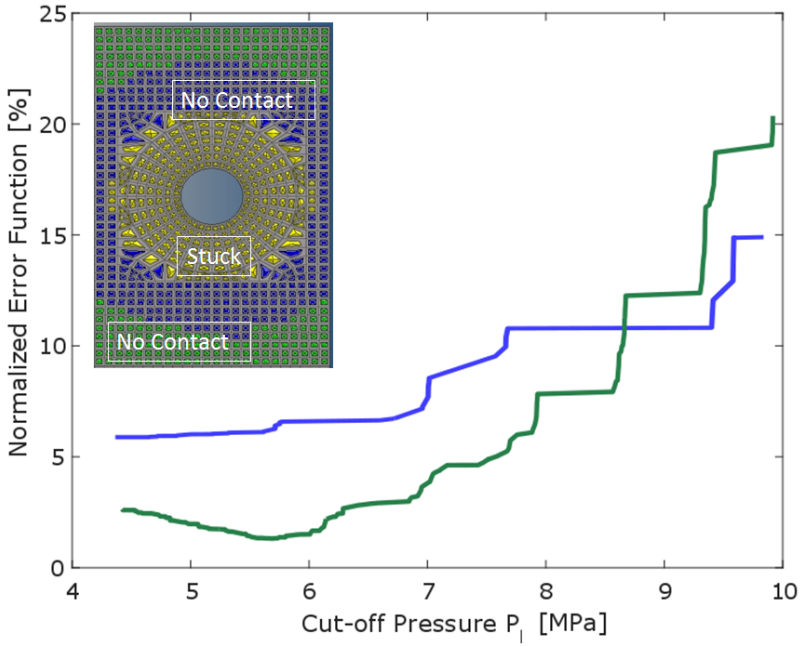

Figure 12: Objective function evaluation for various cut-off pressures for both implementations of the single parameter inverse method: (blue) three contact conditions and (green) two contact conditions

5 CONCLUSIONS

A single parameter inverse method is developed in this research to update contact definitions in a linearized finite element model of a jointed structure to match with experimental modal data. A nominal finite element model of the structure is developed and a nonlinear static preload analysis is completed to estimate the normal contact pressures at the bolted interface. A single parameter, termed the cut-off pressure, is then used to systematically adjust the constraint conditions at the element faces in the interface. Three conditions are utilized in this study: no contact, sliding and stuck. The no contact condition does not enforce any constraints to the elements and hence allows for unrestricted motion in all degrees of freedom. The sliding condition enforces constraints to the displacements in the normal direction, but not in the tangential motion. The stuck condition restricts motion in all degrees of

freedom relative to the node-face pair. The inverse method adjusts the contact constraint in the finite element model using only the value of the cut-off pressure variable and whether or not the predicted normal contact pressures are above or below.

Two implementations of the inverse method are studied. The first assigns no contact for elements with zero pressure, sliding for those less than the cut-off value but greater than zero, and stuck for those with pressures greater than the cut-off value. The second implementation is similar to the first, but instead eliminates the possibility of sliding contact for normal pressures less than the cut-off and enforcing no contact instead. For the C-shape beam system studied in this work, excellent agreement is obtained for the second implementation and the error summed across the first six elastic modes is $< 3\%$. The second approach outperforms the first since there are two "clapping" modes that open and close the interface and need the ability to release the contact constraints in the normal direction. The single parameter inverse method combines model updating approaches, test data, and physical understanding of mode shapes to identify the appropriate contact area within a linearized structural dynamics model. Because of the good agreement obtained from a relatively simple structure, this approach could be used with confidence to explore higher-fidelity models of jointed structures.

Future studies could build on this work by including damping and frictional contact to account for other important physical phenomena in jointed structures with the objective of matching test data with high accuracy. Such a technique would provide greater insight into the physics occurring within frictional interfaces during vibration. In addition, a discrete optimization routine would benefit this approach in order to avoid evaluating the model for a large number of discrete cut-off pressure values and thus more quickly reach the minimum value of the objective function. The need for optimization routines in comparison to open-loop objective function evaluation becomes especially prevalent when increasing the mesh refinement, which can result in a single iteration runtime on the order of minutes or hours.

ACKNOWLEDGMENTS

This research was conducted at the 2017 Nonlinear Mechanics and Dynamics (NOMAD) Research Institute supported by Sandia National Laboratories. Sandia National Laboratories is a multimission laboratory managed and operated by National Technology and Engineering Solutions of Sandia, LLC., a wholly owned subsidiary of Honeywell International, Inc., for the U.S. Department of Energy's National Nuclear Security Administration under contract DE-NA-0003525.

REFERENCES

[1] **Mottershead, J.** and **Friswell, M.**, *Model Updating In Structural Dynamics: A Survey*, Journal of Sound and Vibration, Vol. 167, No. 2, pp. 347–375, 1993.

[2] **Ewins, D. J.**, *Exciting Vibrations: The Role of Testing in an Era of Supercomputers and Uncertainties*, Meccanica, Vol. 51, No. 12, pp. 3241–3258, 2016.

[3] **Nobari, A. S., Robb, D. A.** and **Ewins, D. J.**, *Model Updating and Joint Identification Methods - Applications, Restrictions and Overlap*, International Journal of Analytical and Experimental Modal Analysis, Vol. 8, pp. 93–105, 1993.

[4] **Kim, T. R., Wu, S. M.** and **Eman, K. F.**, *Identification of Joint Parameters for a Taper Joint*, Journal of Engineering for Industry, Vol. 111, No. 3, pp. 282, Aug 1989.

[5] **Ehmann, K. F., Ehmann, K. F.** and **Wu, S. M.**, *Identification of Joint Structural Parameters Between Substructures*, Journal of Manufacturing Science and Engineering, Vol. 113, No. 4, pp. 419, Nov 1991.

[6] **Mottershead, J. E.** and **Weixun, S.**, *Correction of Joint Stiffnesses and Constraints For Finite Element Models in Structural Dynamics*, Journal of Applied Mechanics, Transactions ASME, Vol. 60, No. 1, pp. 117–122, Mar 1993.

[7] **Mottershead, J., Friswell, M., Ng, G.** and **Brandon, J.**, *Geometric Parameters For Finite Element Model Updating of Joints and Constraint*, Mechanical Systems and Signal Processing, Vol. 10, No. 2, pp. 171–182, Mar 1996.

[8] **LI, W.**, *A New Method For Structural Model Updating and Joint Stiffness Identification*, Mechanical Systems and Signal Processing, Vol. 16, No. 1, pp. 155–167, Jan 2002.

[9] **Adel, F., Shokrollahi, S., Jamal-Omidi, M.** and **Ahmadian, H.**, *A Model Updating Method For Hybrid Composite/Aluminum Bolted Joints Using Modal Test Data*, Journal of Sound and Vibration, Vol. 396, pp. 172–185, May 2017.

[10] **Brake, M. R. W., Stark, J. G., Smith, S. A., Lancereau, D. P. T., Jerome, T. W.** and **Dossogne, T.**, In Situ Measurements of Contact Pressure for Jointed Interfaces During Dynamic Loading Experiments, pp. 133–141, Springer International Publishing, Cham, 2017.

[11] **Marshall, M. B., Lewis, R.** and **Dwyer-Joyce, R. S.**, *Characterisation of Contact Pressure Distribution in Bolted Joints*, Strain, Vol. 42, No. 1, pp. 31–43, Feb 2006.

[12] **Segalman, D. J.**, *A Four-Parameter Iwan Model for Lap-Type Joints*, Journal of Applied Mechanics, Vol. 72, No. 5, pp. 752, 2005.

[13] **Allen, M. S., Lacayo, R. M.** and **Brake, M. R.**, *Quasi-static Modal Analysis based on Implicit Condensation for Structures with Nonlinear Joints*.

[14] **Sellgren, U.** and **Olofsson, U.**, *Application of a Constitutive Model For Micro-slip in Finite Element Analysis*, Computer Methods in Applied Mechanics and Engineering, Vol. 170, No. 1, pp. 65–77, Feb 1999.

[15] **Flicek, R. C., Ramesh, R.** and **Hills, D. A.**, *A Complete Frictional Contact: The Transition From Normal Load to Sliding*, International Journal of Engineering Science, Vol. 92, No. February 2017, pp. 18–27, 2015.

[16] **Johnson, K. L.**, Contact Mechanics, 1985.

[17] **Motosh, N.**, *Development of Design Charts for Bolts Preloaded up to the Plastic Range*, Vol. 98, pp. 849, Jan 1976.

[18] **Bickford, J. H.**, *An Introduction to the Design and Behavior of Bolted Joints*, 1995.